






# Field Model Identification and Control of a Mobile Electromagnet for Remote Actuation of Soft Robots

Alessandro Riccardi , Guilherme P. Furtado , Jakub Sikorski , Marilena Vendittelli , *Member, IEEE*,  
and Sarthak Misra , *Senior Member, IEEE*

**Abstract**—The actuation of miniaturized robots through external magnetic fields has great potential for medical applications. The controllability properties of the miniaturized robots are affected by magnetic field generation modality. In this work, the magnetic field of a mobile electromagnet, notably capable to generate a desired magnetic field in large 3D workspaces, has been identified first. Then, a control model of the field generation system has been developed to produce a desired magnetic field designed to generate a locomotion gait in a legged miniaturized robot. Preliminary experiments prove the viability of the approach.

**Index Terms**—Medical robots and systems, micro/nano robots, magnetic devices, robot task control, modeling, control, and learning for soft robots.

## I. INTRODUCTION

THE use of external magnetic fields for remote actuation has been widely studied for potential applications within the domain of medical robotics [1], [2]. In particular, magnetic actuation finds application in steering control of miniaturized, untethered agents, intended to be deployed within the remote areas of the human body [3]. Examples of such agents involve

Manuscript received 2 January 2023; accepted 4 May 2023. Date of publication 29 May 2023; date of current version 6 June 2023. This letter was recommended for publication by Associate Editor K. Rabenoroosa and Editor J. Burgner-Kahrs upon evaluation of the reviewers' comments. This work was supported by the Netherlands Organization for Scientific Research through Innovational Research Incentives Scheme – VIDI: SAMURAI Project under Grant 14855. This study was conceived by Guilherme Phillips Furtado, who tragically passed away during the preparation of this manuscript. The authors dedicate this manuscript in his loving memory. (Alessandro Riccardi and Guilherme P. Furtado contributed equally to this work. This research was conducted during Alessandro Riccardi's time at the Surgical Robotics Laboratory of the University of Twente) (Corresponding author: Alessandro Riccardi.)

Alessandro Riccardi is with the Delft Center for Systems and Control, Delft University of Technology, 2628CD Delft, The Netherlands (e-mail: a.riccardi@tudelft.nl).

Guilherme P. Furtado was with the Surgical Robotics Laboratory, Department of Biomechanical Engineering, University of Twente, 7500AE Enschede, The Netherlands (e-mail: g.phillipsfurtado@utwente.nl).

Jakub Sikorski and Sarthak Misra are with the Surgical Robotics Laboratory, Department of Biomechanical Engineering, University of Twente, 7500AE Enschede, The Netherlands, and also with the Surgical Robotics Laboratory, Department of Biomedical Engineering, University of Groningen and University Medical Center Groningen, 9713GZ Groningen, The Netherlands (e-mail: j.sikorski@utwente.nl; s.misra@utwente.nl).

Marilena Vendittelli is with the Department of Computer, Control and Management Engineering, Sapienza University of Rome, 00185 Rome, Italy (e-mail: vendittelli@diag.uniroma1.it).

This letter has supplementary downloadable material available at <https://doi.org/10.1109/LRA.2023.3280814>, provided by the authors.

Digital Object Identifier 10.1109/LRA.2023.3280814

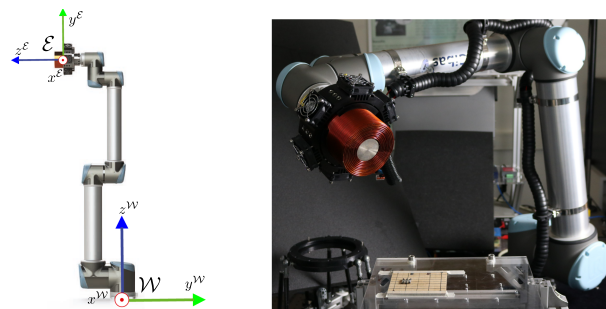


Fig. 1. On the left, the ARMM system, comprising the electromagnet mounted on the end effector of a UR10 manipulator, and the reference frames  $\mathcal{W}$ , fixed at the robot base, and  $\mathcal{E}$ , moving with the electromagnet. The picture on the right shows a close-up view of the electromagnet and the setup used in the experiments described in Section IV.

helical miniaturized swimmers [4], [5], flagellated miniaturized robots [6], [7] and endoscopic capsules [8]. More recently, the progresses in materials science have given raise to new classes of untethered, milli-/micro-scale magnetic soft robots, capable of bioinspired motion in small scales [9], [10], [11]. Various systems using external magnetic fields for the actuation of untethered agents have been presented in the literature, see e.g. [10], [12].

This letter concerns a class of magnetic actuation systems based on mobile electromagnets. Magnetic actuation requires tracking of a reference field that is mainly performed through arrays of fixed [13] or semi-mobile electromagnets [5], [14], for which field reproduction accuracy has been assessed in several studies [1], [15], but they have a limited workspace. Permanent magnets are also used for a limited set of applications that include rotating miniaturized swimmers, but they are not suited for catheters where much stronger fields are required. In this context, the ARMM [16] system, a mobile electromagnet whose mobility is provided by a 6DoF serial manipulator (see Fig. 1), has some advantages over both arrays of electromagnets and permanent magnets, possessing an extended workspace and strong field generation.

Mobile electromagnets for magnetic field tracking are quite rare [2] and, to the best of our knowledge, magnetic field tracking has not been performed yet with systems like ARMM, with a coil mounted on a manipulator, which significantly enlarges the workspace available for magnetic actuation. The original

control architecture of the ARMM was designed for the actuation of magnetic catheters, and its strengths and limitations have been analyzed in [17]. Specifically, the magnetic field actuation produced by the original control design of the ARMM was intended to produce fields along the longitudinal axis of the coil, for catheters steering. Despite the promising results, this approach was intrinsically limiting the magnetic actuation capabilities of the system, assuming the magnetic field to be a vector instead of a field developing in a three-dimensional space. The work presented here aims to fully exploit the magnetic actuation capabilities of the ARMM system. To this end, the dynamic model of the mobile electromagnet is first determined, then a control law that minimizes a cost index trading off the tracking error and the control effort is provided.

On one hand, by relating the multipole expansion model to the joint configuration of the manipulator and current of the coil, we provide a control model of the field suitable for the design of feedback controllers allowing remote actuation of magnetic soft robots. The actuation of these miniaturized robots usually requires an array of electromagnets to be actuated, while rotating permanent magnets are not suited for their actuation. On the other hand, the proposed approach mitigates the limitation of a single coil in producing fast vertical rotating fields, usually produced by rotating permanent magnets. Specifically, we show how to produce vertical rotating fields with a mobile electromagnet that can not rotate on its transversal axis.

The identification of the magnetic field model is performed through a nonlinear regression applied to the spherical multipole expansion [15]. A differential model of the field is then obtained as a linear parameter varying (LPV) system [18], allowing for the application of general control strategies. In particular, an optimal control problem is formulated to take into account actuation and environmental constraints, and a solution based on the Parameter-Dependent Riccati Equation (PDRE) is proposed. This control approach represents a variation of the tracking technique based on the State-Dependent Riccati Equation (SDRE) [19]. In this work, the SDRE is used to effectively track a reference magnetic field with a mobile electromagnet while avoiding obstacles in the workspace.

The identified field model is experimentally validated and the potential of the control method is demonstrated through the actuation of a legged magnetic soft robot, the Hexapod [20], belonging to a category of miniaturized robots which usually require an array of electromagnets to be actuated [13], [14].

The main contributions of the work can be summarized in: the methodological approach proposed to determine the field control model enabling the design of different feedback control schemes, according to tasks and constraints to be satisfied and to the information available for feedback; the identification of the magnetic field parameters for the ARMM system.

The letter is organized as follows. The dynamic model of the mobile electromagnet is determined in Section II. Based on this model, a control law is designed in Section III. Experimental results are discussed in Section IV to estimate the parameters of the model and to validate its accuracy, test the control architecture, and perform the remote actuation of the legged magnetic soft robot Hexapod. Concluding remarks and future work directions are drawn in Section V.

## II. MODELLING OF A MOBILE ELECTROMAGNET

The mobile electromagnet employed in this study is the Advanced Robotics for Magnetic Manipulation (ARMM) system shown in Fig. 1. It comprises of a mobile electromagnet (Wijdeven BV, Oirschot, The Netherlands) mounted on the end effector of a UR10 (Universal Robots, Odense, Denmark) collaborative robot, through which its pose in space is controlled. The electromagnetic coil of the ARMM system is powered using a Xenus XEL-230-40 current controller. Further details about the system can be found in [16]. This section presents the system modeling for control design.

The field generated by the magnet can be modeled using quasi-static assumptions [21] by assuming a linear dependence between the field and the current that powers the coil, within the saturation region of the core. The distribution of the field can then be represented by using a unit current field  $\mathbf{B}_U^\mathcal{E} \in \mathbb{R}^3$ , expressed in the electromagnet body frame  $\mathcal{E}$ . We model  $\mathbf{B}_U^\mathcal{E}$  using the multipole expansion technique presented in [15]:

$$\mathbf{B}_U^\mathcal{E}(\mathbf{p}^\mathcal{E}) = \sum_{n=1}^N \left( \left( C_n^2 \xi P_n' - C_n^1 P_n \right) \hat{\mathbf{p}}^\mathcal{E} - C_n^2 P_n' \hat{\mathbf{z}}_s \right) \quad (1)$$

$$C_n^1 = -\frac{(n+1)B_n}{\|\mathbf{p}^\mathcal{E}\|^{n+2}}, \quad C_n^2 = \frac{B_n}{\|\mathbf{p}^\mathcal{E}\|^{n+2}}, \quad \xi = \hat{\mathbf{z}}_s \cdot \hat{\mathbf{p}}^\mathcal{E}. \quad (2)$$

The point  $\mathbf{p}^\mathcal{E} \in \mathbb{R}^3$  corresponds to a location expressed in  $\mathcal{E}$ , while  $\hat{\mathbf{z}}_s \in \mathbb{R}^3$  is the unit vector indicating the electromagnet longitudinal axis of symmetry.  $P_n(\xi)$  and  $P_n'(\xi)$  are, respectively, the Legendre polynomial of order  $n$  and its first derivative, and  $N \in \mathbb{N}$  is the order of the multipole expansion trade-off. In this work, the order of expansion that provides the best tradeoff between complexity and accuracy of the cylindrical source through multipole expansion has been experimentally found to be equal to 3. The coefficients  $B_n$ , with  $n$  odd, have also been identified experimentally. The  $B_n$ 's corresponding to even values of  $n$  have been set to zero to ensure the symmetry of the field. Details are provided in Section IV.

For control design purposes, it is convenient to express the unit current field model (1) in world coordinates. Let  $\mathcal{W}$  denote the world reference frame, placed as in Fig. 1,  $\mathbf{B}^\mathcal{W} \in \mathbb{R}^3$  and  $\mathbf{p}_t^\mathcal{W} \in \mathbb{R}^3$  respectively the magnetic field generated by the ARMM system and a target point in space (where the field value should be controlled), both in world frame coordinates. The field can be expressed as a function of the current  $i_e \in \mathbb{R}$  running through the electromagnet and of the pose  $\mathbf{H}_\mathcal{E}^\mathcal{W} \in \text{SE}(3)$  of the electromagnet reference frame with respect to the world reference frame  $\mathcal{W}$ . The pose  $\mathbf{H}_\mathcal{E}^\mathcal{W}$  is determined by the value of the joint variables  $\mathbf{q} \in \mathbb{R}^6$ , defining the configuration of the UR10, and it is parametrized by the position  $\mathbf{p}_e^\mathcal{W}(\mathbf{q}) \in \mathbb{R}^3$  of the body frame origin and its orientation, with respect to  $\mathcal{W}$ , described by a set of Euler angles  $\gamma_e^\mathcal{W}(\mathbf{q}) \in \mathbb{S}^3$ .

The value of  $\mathbf{B}^\mathcal{W}$  at the target point  $\mathbf{p}_t^\mathcal{W}$  depends on the pose of the electromagnet  $[\mathbf{p}_e^\mathcal{W} \gamma_e^\mathcal{W}]^T$ , on the current  $i_e$  through it, and clearly on the considered target point. Noting that the pose defined is determined by the configuration  $\mathbf{q}(t)$  of the manipulator, the value of the field at a given point will be dependent on a set of measurable time-varying parameters

$\theta(t) = [\mathbf{q}^T(t) \quad i_e(t) \quad \mathbf{p}_t^{\mathcal{W}T}(t)]^T$ , i.e. the field is expressed as the function  $\mathbf{B}^{\mathcal{W}}(\theta(t))$ . Then, differentiating  $\mathbf{B}^{\mathcal{W}}(\theta(t))$  with respect to  $\theta(t)$  we obtain the differential model of the field, which takes the form of a Linear Parameter Varying (LPV) dynamic model [22]:

$$\begin{aligned} \frac{d\mathbf{B}^{\mathcal{W}}}{dt} &= \frac{\partial \mathbf{B}^{\mathcal{W}}}{\partial \mathbf{p}_e^{\mathcal{W}}} \dot{\mathbf{p}}_e^{\mathcal{W}} + \frac{\partial \mathbf{B}^{\mathcal{W}}}{\partial \gamma_e^{\mathcal{W}}} \dot{\gamma}_e^{\mathcal{W}} + \frac{\partial \mathbf{B}^{\mathcal{W}}}{\partial i_e} \dot{i}_e + \frac{\partial \mathbf{B}^{\mathcal{W}}}{\partial \mathbf{p}_t^{\mathcal{W}}} \dot{\mathbf{p}}_t^{\mathcal{W}} \\ &= \mathbf{J}_{\mathbf{p}_e^{\mathcal{W}}}^{\mathbf{B}^{\mathcal{W}}} \frac{\partial \mathbf{p}_e^{\mathcal{W}}}{\partial \mathbf{q}} \dot{\mathbf{q}} + \mathbf{J}_{\gamma_e^{\mathcal{W}}}^{\mathbf{B}^{\mathcal{W}}} \frac{\partial \gamma_e^{\mathcal{W}}}{\partial \mathbf{q}} \dot{\mathbf{q}} + \mathbf{B}_U^{\mathcal{W}} \dot{i}_e + \mathbf{J}_{\mathbf{p}_t^{\mathcal{W}}}^{\mathbf{B}^{\mathcal{W}}} \dot{\mathbf{p}}_t^{\mathcal{W}} \\ &= \left[ \left( \mathbf{J}_{\mathbf{p}_e^{\mathcal{W}}}^{\mathbf{B}^{\mathcal{W}}} \mathbf{J}_L + \mathbf{J}_{\gamma_e^{\mathcal{W}}}^{\mathbf{B}^{\mathcal{W}}} \mathbf{J}_A \right) \quad \mathbf{B}_U^{\mathcal{W}} \right] \begin{bmatrix} \dot{\mathbf{q}} \\ \dot{i}_e \end{bmatrix} + \mathbf{J}_{\mathbf{p}_t^{\mathcal{W}}}^{\mathbf{B}^{\mathcal{W}}} \dot{\mathbf{p}}_t^{\mathcal{W}} \\ \dot{\mathbf{x}} &= \mathbf{B}(\theta(t)) \mathbf{u} + \mathbf{D}(\theta(t)) \mathbf{d}, \end{aligned} \quad (3)$$

where  $\mathbf{x} = \mathbf{B}^{\mathcal{W}}(\theta(t))$  is the state of the system,  $\mathbf{u} = [\dot{\mathbf{q}}^T \quad \dot{i}_e]^T$  is the control input, and  $\mathbf{d} = \dot{\mathbf{p}}_t^{\mathcal{W}}$  is an external, measurable and limited disturbance acting on the nominal dynamics, while  $\mathbf{J}_L$  and  $\mathbf{J}_A$  are respectively the linear and angular Jacobian of the manipulator. It is worth noticing that the dependence of this dynamics on the set of time-varying parameters  $\theta(t)$  is nonlinear. The differential model developed in (3) including the Jacobians, as well as the expression of the field in the reference frames  $\mathcal{E}$  and  $\mathcal{W}$ , are provided in symbolic closed-form as the result of the execution of the code available at [23].

The rationale for interpreting (3) as an LPV system is to cast the control model that it encompasses in a class of systems suitable for direct application of the systematic control design method based on state-dependent Riccati equation illustrated in the next section. In fact, the differential model of the field given by (3) can be interpreted as the kinematics of the magnetic field generation task. As such, kinematic control techniques typically used for robotic manipulators could also be adapted to this application. The main reasons for adopting SDR-based control design consist of its generality, design flexibility, and ease of implementation. In addition, the closed-form expression of the controller derived in the next section makes it suitable for real-time applications.

### III. FIELD MODEL CONTROLLER

We use the model (3) to formulate a control strategy based on optimal control theory [24]. The nominal plant, not affected by  $\dot{\mathbf{p}}_t^{\mathcal{W}}$ , interpreted here as a disturbance, will be considered for control design. The optimal tracking problem can be formulated as follows.

Given the field reference  $\mathbf{r} = \mathbf{B}_r^{\mathcal{W}}(\mathbf{p}_t^{\mathcal{W}}(t))$  at the target point  $\mathbf{p}_t^{\mathcal{W}}(t)$ , consider the infinite horizon minimization problem of the cost index:

$$J(\mathbf{e}, \mathbf{u}, \theta(t)) = \frac{1}{2} \int_{t_0}^{\infty} [\mathbf{e}^T \mathbf{Q}(\theta(t)) \mathbf{e} + \mathbf{u}^T \mathbf{R}(\theta(t)) \mathbf{u}] dt \quad (4)$$

subject to the differential constraint:

$$\dot{\mathbf{e}} = \dot{\mathbf{r}} - \dot{\mathbf{x}}. \quad (5)$$

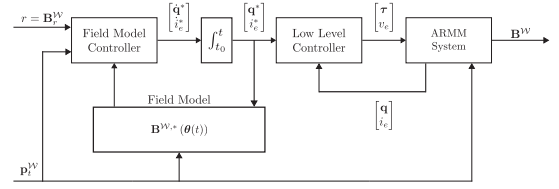


Fig. 2. Open loop implementation of the control law (6), which corresponds to a control-based planning architecture generating references for the low-level ARMM controller.

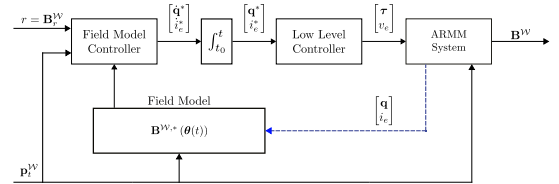


Fig. 3. Implementation of the control law (6) with feedback from the robot configuration and electromagnet current.

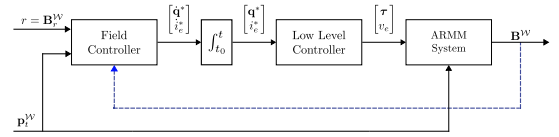


Fig. 4. Implementation of the control law (6): loop closure from the field at the target.

In the above (4),  $\mathbf{e} = \mathbf{r} - \mathbf{x} \in \mathbb{R}^3$  is the field tracking error and  $\mathbf{u} \in \mathbb{R}^7$  the control input. The weighting matrices  $\mathbf{Q}(\theta(t)) \geq 0$ ,  $\mathbf{R}(\theta(t)) > 0$  are symmetric and of suitable dimensions.

We propose a control law that aims to minimize the cost index (4), and which is inspired by the SDR tracking technique for nonlinear autonomous systems [19]. Under the hypothesis that  $B(\theta(t))$  is bounded in norm and stabilizable, and that  $Q(\theta(t))^{\frac{1}{2}}$  (Cholesky decomposition of  $\mathbf{Q}(\theta(t))$ ) is detectable [19], the control that allows to track the reference field  $\mathbf{r} = \mathbf{B}_r^{\mathcal{W}}$  takes the form:

$$\mathbf{u} = -\mathbf{R}(\theta(t))^{-1} \mathbf{B}(\theta(t))^T \mathbf{P}(\theta(t)) \mathbf{e}. \quad (6)$$

In the above equation  $\mathbf{P}(\theta(t)) > 0$  can be obtained iteratively as the result of the integration of the Parameter-Dependent Differential Riccati Equation defined as:

$$\begin{aligned} \dot{\mathbf{P}}(\theta(t)) &= \\ & \mathbf{P}(\theta(t)) \mathbf{B}(\theta(t)) \mathbf{R}(\theta(t))^{-1} \mathbf{B}(\theta(t))^T \mathbf{P}(\theta(t)) - \mathbf{Q}(\theta(t)). \end{aligned} \quad (7)$$

It is worth noticing that the above hypotheses on the matrices  $B(\theta(t))$  and  $Q(\theta(t))$  correspond to the stabilizability and detectability conditions that, in the particular case under study, reduces to the requirement that both matrices have rank equal to 3, i.e. the dimension of the task. The conditions are generically satisfied because  $B(\cdot)$  is a  $3 \times 7$  matrix that might lose rank at singular configurations that depend on the architecture of the manipulator and its interaction with the field. Further study is required to identify such singular configurations which are not trivial to determine analytically. Note, however, that the

cost index (4) determines a trade-off between task accuracy and control effort, typically diverging in close proximity of singularities. We, therefore, claim the avoidance of singularities in our setting. The definition of weighting matrix  $Q^{\frac{1}{2}}(\cdot)$  is left to control design; in the next section we propose to use this matrix to weight the distance between the electromagnet and workspace obstacles and in this case, it can lose rank only when an obstacle collides with a control point on the manipulation system but such a situation is prevented in our setting. Depending on the available feedback information, the control law (6) can be implemented in different ways and with different objectives. In this work we have implemented the open-loop architecture of Fig. 2, thus providing a control-based planning method. In this case, the predicted value of the field  $\mathbf{B}^{\mathcal{W},*}(\boldsymbol{\theta}(t))$  at the target is computed on the basis of the parameter value  $\boldsymbol{\theta}(t) = [\mathbf{q}^*(t) \ i_e^*(t) \ \mathbf{p}_t^{\mathcal{W}}(t)]^T$ , where  $\mathbf{q}^*(t)$  and  $i_e^*(t)$  are determined by intergration of the control  $\mathbf{u}$  provided by (6), and  $\mathbf{p}_t^{\mathcal{W}}(t)$  is a properly designed target trajectory along which the reference field is capable to generate a desired motion of the miniaturized robot. The next section illustrates the identification of  $\mathbf{B}^{\mathcal{W},*}(\boldsymbol{\theta})$  and its experimental validation.

In all control schemes, the set-point signals  $\mathbf{q}^*(t)$  and  $i_e^*(t)$ , determined by the control law (6), are sent to the low-level controller of the ARMM system that computes the actuation torque  $\boldsymbol{\tau}$  and the electromagnet controlling voltage  $v_e$ . The resulting actual values of the system variables are denoted as  $(\mathbf{B}^w, \mathbf{q}, i_e)$ , over which two nested loops can be closed. Specifically, the first loop is easily closed using measured values of the variables of the ARMM system, as illustrated in Fig. 3. A more robust way to implement this law is by measuring the magnetic field at the target as in Fig. 4, although this measure is not easy to obtain, or by closing the loop from the miniaturized robot position. This last method, however, requires appropriate sensory equipment and elaboration to retrieve position information, and a motion model of the agent to be manipulated, which is beyond the scope of this letter.

#### A. Obstacle Avoidance

The weighting matrices  $\mathbf{Q}$  and  $\mathbf{R}$  can be defined as diagonal matrices partitioned according to the structure of  $\mathbf{x}$  and  $\mathbf{u}$ :

$$\mathbf{Q}(\boldsymbol{\theta}(t)) = K_1 f_o(\boldsymbol{\theta}(t)), \quad \mathbf{R}^{-1}(\boldsymbol{\theta}(t)) = K_2 f_o(\boldsymbol{\theta}(t)) \quad (8)$$

where  $(K_1 \in \mathbb{R}^{3 \times 3})$ ,  $(K_2 \in \mathbb{R}^{7 \times 7})$ , and  $f_o(\boldsymbol{\theta}(t))$  is the obstacle avoidance function defining the artificial potential which will be used to prevent collisions with the environment. In the proposed experiments,

$$f_o(\boldsymbol{\theta}(t)) = (k_o \|\mathbf{p}_c(\boldsymbol{\theta}(t)) - \mathbf{p}_o\|)^{k_p}. \quad (9)$$

The general concept behind this formulation is the following: as a control point  $\mathbf{p}_c(\boldsymbol{\theta}(t))$  on the body of the ARMM and the closest obstacle point  $\mathbf{p}_o$  in the workspace become closer, the value of function  $f_o(\boldsymbol{\theta}(t))$  decreases. In that way, gains in matrix  $\mathbf{Q}(\boldsymbol{\theta}(t))$  tend to zero and the controller will relax the reference tracking objective. Meanwhile, terms in  $\mathbf{R}(\boldsymbol{\theta}(t))$  will increase, and with them the cost of specific control actions according to the matrix  $K_2$ . This will favor the use of inputs  $\mathbf{u}$  that steer

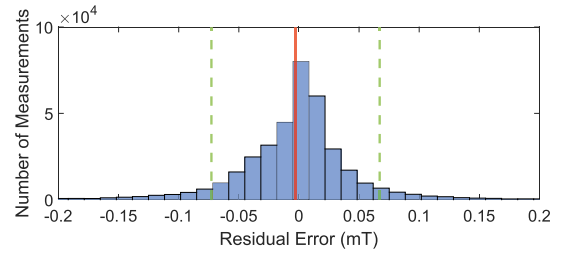


Fig. 5. Histogram of residual errors expressed in  $mT$  for a 3-th order estimation. They are distributed according to a Gaussian model, with mean  $\mu = -2.83 \cdot 10^{-3}$  (red solid line) and variance  $\sigma = 6.99 \cdot 10^{-2}$  (green dashed lines).

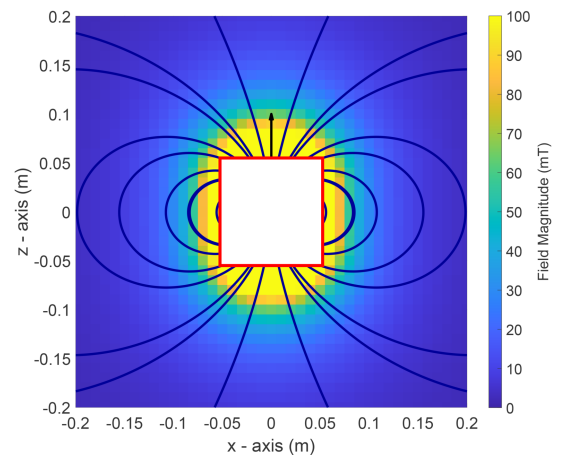


Fig. 6. Streamlines of the field model for a current  $I_e = 15$  A with field magnitude expressed in  $mT$ . For this maximum current, the electromagnet can provide, in a range of 5 cm around it, field intensities that are over 75  $mT$ .

the manipulator (i.e. the control point) away from the closest obstacle. One useful feature of this approach is that the obstacle set can be updated in real-time to account for moving objects or operators in the workspace, allowing the robot to operate in a collaborative environment. This is however beyond the scope of this work and will be the subject of further study.

The above strategy can guarantee collision avoidance for the electromagnet only. To avoid collisions of the whole system body reactive methods based on potential fields can be applied, with the limitations associated with the presence of local minima in which they can get stuck. A valuable alternative would be to devise a task and motion planning method that provides a feasible (i.e., with an associated collision-free Cartesian trajectory of the electromagnet) task and whole-body collision-free motion for the manipulator. To our best knowledge, such a planning method is not available in the literature and could be an interesting topic for future study.

## IV. EXPERIMENTAL RESULTS

This section reports on the experiments performed to identify and validate the magnetic field model of (1) and its use for the actuation of a soft, six-legged, miniaturized robot.

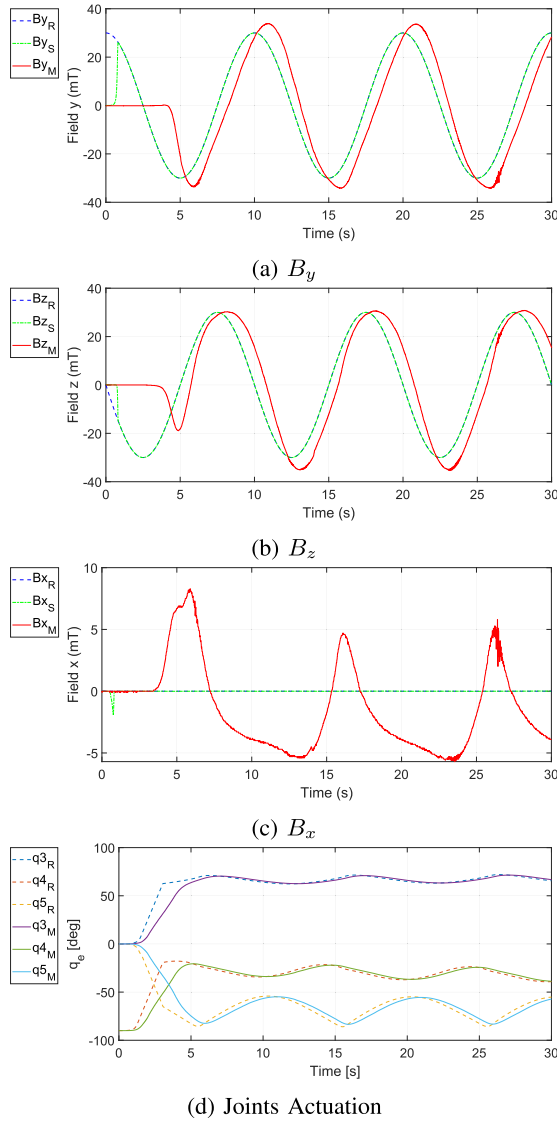


Fig. 7. Rotating Field Actuation - In Figs. (a)–(b)–(c) are represented the reference field  $B_{\cdot,R}$ , the field produced in the control simulation  $B_{\cdot,S}$ , which is used as a reference for the low-level controller, and the measured field  $B_{\cdot,M}$  produced in the experiments. In Fig. (d) are represented the joint references  $q_{\cdot,R}$  for the low-level controller and the measured joint variables  $q_{\cdot,M}$  for joints  $q_3$ ,  $q_4$ , and  $q_5$ .

### A. Field Model Identification

Using the ARMM system in Fig. 1, an estimate of coefficients  $B_n$  in (2) has been obtained through a set of 3-D field measurements acquired in 62566 different points in front of the coil using the 3MH3A-500 Teslameter (Senis AG, Baar, Switzerland) mounted on a UR5 (Universal Robots, Odense, Denmark) manipulator for accurate positioning. The nonlinear least squares estimate aims to minimize the sum of the squares of the residuals between the measured field and the field model. The distribution of the residuals of the estimate is reported in Fig. 5. The streamlines of the resulting field model are shown in Fig. 6. The most suitable trade-off between accuracy and performance of the field model has been obtained with a third order model,

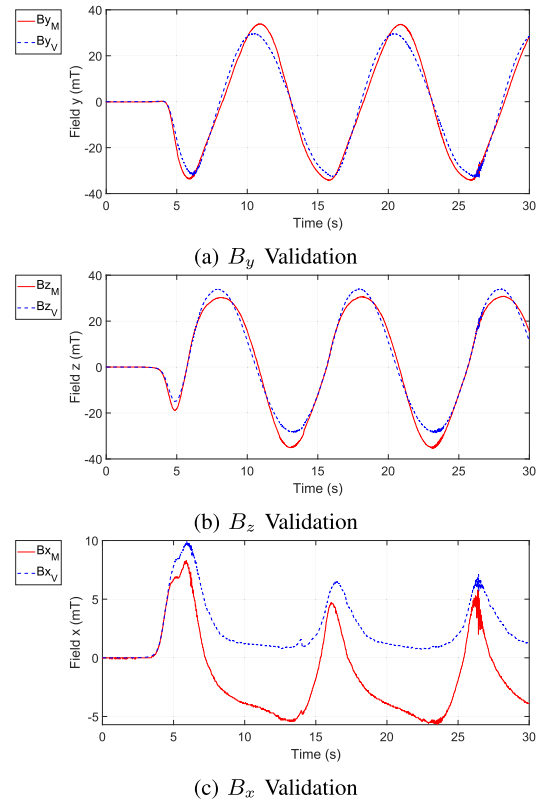


Fig. 8. Model Validation - The measured field is denoted by  $B_{\cdot,M}$  and the field model computed with measured joint variables by  $B_{\cdot,V}$

with coefficients  $B_1 = 2.0487 \cdot 10^{-6}$  and  $B_3 = 5.1671 \cdot 10^{-10}$ , and even coefficient  $B_2$  set to zero to ensure field symmetry.

### B. Simulations and Control Experiments

To perform the following experiments on the real robot, simulations of the control architecture in Fig. 2 have been performed in MATLAB and Simulink. The resulting joint configuration  $\mathbf{q}^*$  and current  $i_e^*$  have been used as references for the low-level controller of the ARMM system.

The first experiment aims to show the ability of the system to produce a rotating field on the vertical plane while keeping the center of the electromagnet at a safe distance from the target point where the Teslameter is positioned. The produced actuating field has been measured with the Teslameter to validate the field generation accuracy.

In the second experiment, the miniaturized robot Hexapod is actuated by the ARMM system.

1) *Vertical Rotating Field At the Target  $\mathbf{p}_t^w$* : The reference is a vertical rotating field of magnitude  $\|\mathbf{B}_r^w\| = 30$  mT and period of rotation of  $T = 10$  s

$$\mathbf{B}_r^w(t) = \begin{bmatrix} 0 & 0.03 \cos\left(\frac{2\pi}{10}t\right) & 0.03 \sin\left(\frac{2\pi}{10}t\right) \end{bmatrix}^T. \quad (10)$$

To hold the surface of the electromagnet at a distance of at least 2.4 cm from the target position an obstacle avoidance function  $f_o(\theta(t))$  is used. Being the electromagnet contained in a ball of

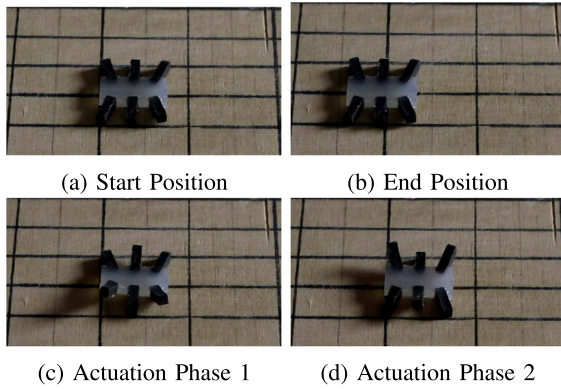


Fig. 9. Hexapod Actuation Experiment. (a)–(b) illustrate the distance traveled by the Hexapod 8.5[mm]. (c)–(d) two different gait phases. On each actuation phase, and alternatively in this case, three legs of the Hexapod are in contact with the ground, and three are raised by the magnetic field defining a semi-circumference which allows it to proceed forward.

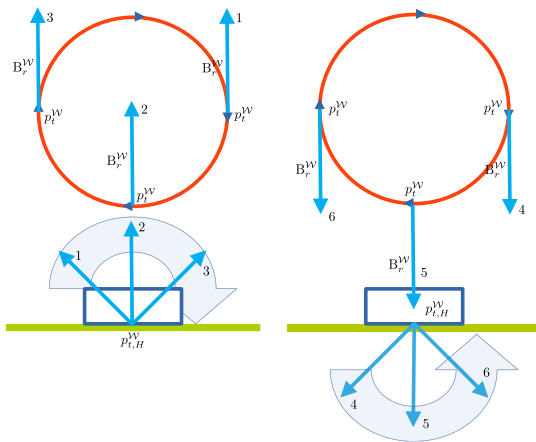


Fig. 10. Actuation field reference and induced actuation field corresponding to Phase 1 (left), Phase 2 (right) of Fig. 9 for the induction of the actuation gait on the Hexapod. The reference field is a vertical vector  $B_r^W$  applied to the target point  $p_t^W$  moving along the sliding circumference in red. The reference vectors  $B_r^W$  are numbered from 1 to 6 to illustrate which effect the field applied in  $p_t^W$  will produce on the Hexapod (dark blue) center in  $p_{t,H}^W$ . The semicircular light-blue arrow represents the direction of rotation of the induced field.

radius 7.6 cm leads to the expression:

$$f_o(\boldsymbol{\theta}(t)) = (10 (\|\mathbf{p}_e^W(\boldsymbol{\theta}(t)) - \mathbf{p}_t^w\| - 0.1))^2 \quad (11)$$

The results of this experiment are illustrated in Fig. 7. The rotating field is reproduced with the correct shape on the  $y-z$  plane with an error in magnitude that is contained at 10%, Fig. 7(a), (b). However, a certain time delay is present and it can be related to the fact that the vector  $[\mathbf{q}^{*T}, i_e^{*T}]^T$ , which is the output of computer simulation, is used as a reference for the low-level controller. This is clear in Fig. 7(d), where joint references are compared with measured values of joint variables. This issue can be solved by implementing the closed-loop control architecture in Fig. 3. Moreover, the field on the  $x$ -axis presents a deviation of 5 mT around zero, Fig. 7(c). This problem is a combination of the actuation delay and model inaccuracies, mainly due to the simplification introduced by the spherical multipole expansion in magnetostatic conditions.

To alleviate the effect of the actuation delay and properly understand the validity of the model, a posteriori validation is performed, comparing the measured field with the field predicted by the model  $\mathbf{B}^{W,*}(\boldsymbol{\theta}(t))$  computed using the measured joint variables resulting from the experiment proposed in Fig. 7. The results in Fig. 8 show, in fact, a greater model accuracy w.r.t. the ones in Fig. 7. The residual error present in Fig. 8 is to be related to the absence of a hysteresis model for the core of the electromagnet, the magnetostatics modeling assumptions, possible millimetric errors in the positioning of the teslameter probe, and from the fact that the electromagnet considered is not an ideal magnet. Modeling accuracy can be further extended using more sophisticated or ad-hoc modeling techniques, however, this will increase the complexity of the resulting controller.

2) *Hexapod Actuation*: To enable motion of the legged miniaturized robot Hexapod [20] shown in Fig. 9, a gait must be generated by a periodic field. The expected trajectory of the target point  $\mathbf{p}_t^W$  must therefore be periodic. This trajectory should be obtained through a planning phase based on a motion generation model for the Hexapod. A rigorous motion generation model of the Hexapod is beyond the scope of this letter and will be the objective of future study.

In this preliminary work, to generate a locomotion gait in the Hexapod a reference field switching between  $[-10, 10]$  mT is assigned along the  $z$ -axis and evaluated at the target  $\mathbf{p}_t^W(t)$  that describes a circumference over the Hexapod, with its center equal to the planned position of the Hexapod on the  $x-y$  plane. Thus, target motion is defined through:

$$\dot{\mathbf{p}}_t^W = \dot{\mathbf{p}}_{t,T}^W + \dot{\mathbf{p}}_{t,H}^W \quad \dot{\mathbf{p}}_{t,H}^W = \begin{bmatrix} -0.9 \cdot 10^{-4} & 0 & 0 \end{bmatrix}^T \quad (12)$$

$$\dot{\mathbf{p}}_{t,T}^W = \begin{bmatrix} 0.15 \left(\frac{2\pi}{10}\right) \cos\left(\frac{2\pi}{10}t\right) & 0 & -0.15 \left(\frac{2\pi}{10}\right) \sin\left(\frac{2\pi}{10}t\right) \end{bmatrix}^T \quad (13)$$

where  $\dot{\mathbf{p}}_{t,H}^W$  is the predicted velocity of the Hexapod and translates the center of the circumference produced by  $\dot{\mathbf{p}}_{t,T}^W$ .

The magnetic actuation is divided in two phases, Fig. 10(c) and (d), which are defined by the value of the switching actuation current and the position of the electromagnet, leading to an alternating movement of the legs of the Hexapod (a gait), producing motion of the miniaturized robot body on a straight line with constant speed. Following the reference field depicted in Fig. 10, the vertical switching magnetic field  $B^W$  applied in  $p_t^W$  produces on the position of the target (Hexapod) a periodic field with a complex pattern. It was not possible with our equipment to measure this field in the exact position of the Hexapod during the experiment illustrated in Fig. 9. Therefore, we have measured the field produced to induce the same locomotion gait for a fixed target position  $p_t^W$  in the start position of Fig. 9. The resulting field along the three axes, as well as the switching current required to produce the actuation, are reported in Fig. 11. Note that, feedback on the robot position could have been closed, in this case, using an external camera to track the hexapod motion. However, the additional effort and complexity of implementing a vision-based closed-loop control were not worth it, because the real challenge is to track the miniaturized robot inside the human

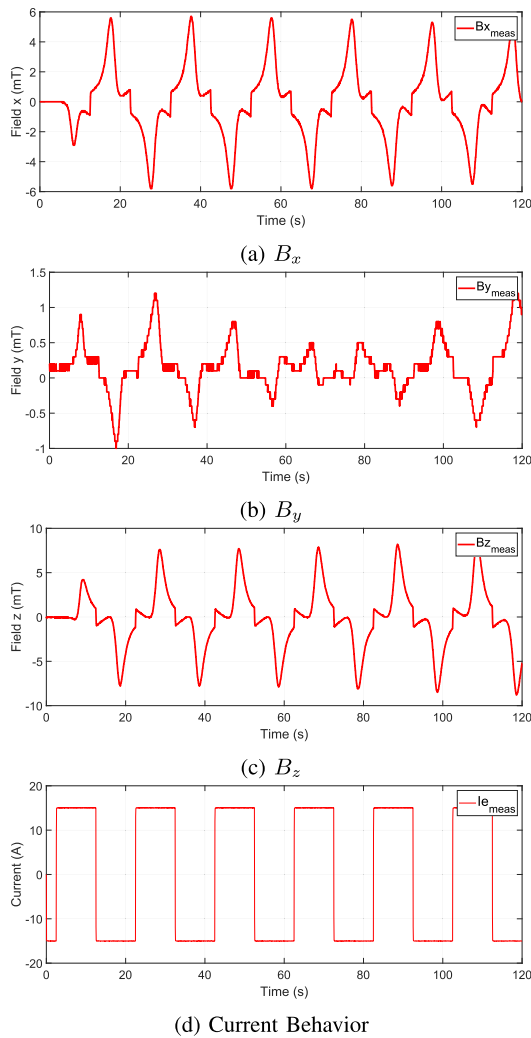


Fig. 11. Measured Hexapod actuation field (a)–(c) and respective switching current (d). This field is the result of the planning proposed in Fig. 10. The current switch is almost instantaneous w.r.t. the time-scale of the Hexapod actuation.

body. The presented preliminary experiments are, instead, based on open-loop gait generation using the field model and control presented in the previous sections. This experiment produced an average speed of the Hexapod of 0.071 mm/s for an actuation time of 120 s, i.e., 8.5 mm distance covered by the Hexapod without any significant lateral deviation. This result is in line with other recent experiments with magnetic soft robots [20], considering that the rotation period of the magnetic field is 10[s]. A movie clip of the experiment is included in the accompanying multimedia material.

## V. CONCLUSION

In this work a model of the electromagnet composing the magnetic manipulation system ARMM has been first identified to be used in a control scheme suitable for solving both planning and control problems. The experimental validation of the field generation system has eventually led to preliminary, promising, experiments in gait generation for magnetically actuated legged miniaturized robots. Future work includes: the development of planning methods for the actuating field, based on motion

models of the miniaturized robots to be actuated; adoption of task control methods to easily exploit the redundancy of the system to avoid joint limits and configuration drifting while executing cyclic trajectories in the Cartesian space; address the obstacle avoidance problem in the whole configuration space including moving obstacles.

## REFERENCES

- [1] J. J. Abbott, E. Diller, and A. J. Petruska, "Magnetic methods in robotics," *Annu. Rev. Control, Robot., Auton. Syst.*, vol. 3, pp. 57–90, 2020.
- [2] Y. Shao, A. Fahmy, M. Li, C. Li, W. Zhao, and J. Sienz, "Study on magnetic control systems of micro-robots," *Front. Neurosci.*, vol. 15, 2021, Art. no. 736730.
- [3] M. Sitti et al., "Biomedical applications of untethered mobile milli/microrobots," *Proc. IEEE Proc. IRE*, vol. 103, pp. 205–224, 2015.
- [4] K. E. Peyer, S. Tottori, F. Qiu, L. Zhang, and B. J. Nelson, "Magnetic helical micromachines," *Chem.—A Eur. J.*, vol. 19, pp. 28–38, 2013.
- [5] Z. Yang, L. Yang, and L. Zhang, "3D visual servoing of magnetic miniature swimmers using parallel mobile coils," *IEEE Trans. Med. Robot. Bionics*, vol. 2, no. 4, pp. 608–618, Nov. 2020.
- [6] V. Magdanz et al., "IRONSpERM: Sperm-templated soft magnetic micro-robots," *Sci. Adv.*, vol. 6, 2020, Art. no. eaba5855.
- [7] V. Magdanz et al., "Impact of segmented magnetization on the flagellar propulsion of sperm-templated microrobots," *Adv. Sci.*, vol. 8, 2021, Art. no. 2004037.
- [8] J. W. Martin et al., "Enabling the future of colonoscopy with intelligent and autonomous magnetic manipulation," *Nature Mach. Intell.*, vol. 2, pp. 595–606, 2020.
- [9] S. Wu, W. Hu, Q. Ze, M. Sitti, and R. Zhao, "Multifunctional magnetic soft composites: A review," *Multifunctional Mater.*, vol. 3, 2020, Art. no. 042003.
- [10] M. Eshaghi, M. Ghasemi, and K. Khorshidi, "Design, manufacturing and applications of small-scale magnetic soft robots," *Extreme Mechanics Lett.*, vol. 44, 2021, Art. no. 101268.
- [11] J. Qi et al., "Recent progress in active mechanical metamaterials and construction principles," *Adv. Sci.*, vol. 9, 2022, Art. no. 2102662.
- [12] Z. Yang and L. Zhang, "Magnetic actuation systems for miniature robots: A review," *Adv. Intell. Syst.*, vol. 2, 2020, Art. no. 2000082.
- [13] M. P. Kummer, J. J. Abbott, B. E. Kratochvil, R. Borer, A. Sengul, and B. J. Nelson, "OctoMag: An electromagnetic system for 5-DOF wireless micromanipulation," *IEEE Trans. Robot.*, vol. 26, no. 6, pp. 1006–1017, Dec. 2010.
- [14] J. Sikorski, I. Dawson, A. Denasi, E. E. G. Hekman, and S. Misra, "Introducing BigMag – A novel system for 3D magnetic actuation of flexible surgical manipulators," in *Proc. IEEE Int. Conf. Robot. Automat.*, 2017, pp. 3594–3599.
- [15] A. J. Petruska, J. Edelman, and B. J. Nelson, "Model-based calibration for magnetic manipulation," *IEEE Trans. Magn.*, vol. 53, no. 7, Jul. 2017, Art. no. 4900206.
- [16] J. Sikorski, C. M. Heunis, F. Franco, and S. Misra, "The ARMM system: An optimized mobile electromagnetic coil for non-linear actuation of flexible surgical instruments," *IEEE Trans. Magn.*, vol. 55, no. 9, 2019, Art. no. 5600109.
- [17] C. M. Heunis, Y. P. Wotte, J. Sikorski, G. P. Furtado, and S. Misra, "The ARMM system - Autonomous steering of magnetically-actuated catheters: Towards endovascular applications," *IEEE Robot. Automat. Lett.*, vol. 5, no. 2, pp. 705–712, Apr. 2020.
- [18] C. Briat, "Linear parameter-varying and time-delay systems," *Anal., Observ., Filtering Control*, vol. 3, pp. 5–7, 2014.
- [19] T. Çimen, "State-dependent riccati equation (SDRE) control: A survey," *IFAC Proc. Volumes*, vol. 41, pp. 3761–3775, 2008.
- [20] V. K. Venkiteswaran, L. F. P. Samaniego, J. Sikorski, and S. Misra, "Bio-inspired terrestrial motion of magnetic soft millirobots," *IEEE Robot. Automat. Lett.*, vol. 4, no. 2, pp. 1753–1759, Apr. 2019.
- [21] J. D. Jackson, *Classical Electrodynamics*. College Park, MD, USA: American Association of Physics Teachers, 1999.
- [22] J. Mohammadpour and C. W. Scherer, *Control of Linear Parameter Varying Systems With Applications*. Berlin, Germany: Springer, 2012.
- [23] A. Riccardi, G. P. Furtado, J. Sikorski, M. Vendittelli, and S. Misra, "The ARMM system - Magnetic field dynamics," [Online]. Available: <https://gitlab.tudelft.nl/ariccardi/the-armm-system-magnetic-field-dynamics.git>
- [24] H. Kwakernaak and R. Sivan, *Linear Optimal Control Systems*. Hoboken, NJ, USA: Wiley, 1972.